OPEN ACCESS

Original research

Magnesium-based bioresorbable flow diverter for intracranial aneurysms: a pilot study of biocompatibility and bioresorption in a rabbit vascular model

Ryo Akiyama ,[1] Akira Ishii ,[2] Natsuhi Sasaki ,[3] So Matsukawa ,[1] Shinichi Yagi ,[4] Hideo Chihara ,[1] Hidehisa Nishi ,[2] Kiyotaka Iwasaki ,[5] Shinichi Sakurai ,[4] Yoshihito Kawamura ,[6] Yoshiki Arakawa [1]

► Additional supplemental material is published online only. To view, please visit the journal online (https://doi.org/10.1136/jnis-2024-022527).

[1]Neurosurgery, Kyoto University Graduate School of Medicine Faculty of Medicine, Kyoto, Japan
[2]Neurosurgery, Juntendo University School of Medicine Graduate School of Medicine, Tokyo, Japan
[3]Neurosurgery, Fukui Red Cross Hospital, Fukui, Japan
[4]Biobased Materials Science, Kyoto Institute of Technology Faculty of Textile Science, Kyoto, Japan
[5]Cooperative Major in Advanced Biomedical Sciences, Waseda University School and Graduate School of Advanced Science and Engineering, Tokyo, Japan
[6]Magnesium Research Center, Kumamoto University, Kumamoto, Japan

Correspondence to
Professor Akira Ishii; ishiiakira@gmail.com

Received 20 September 2024
Accepted 5 November 2024

To cite: Akiyama R, Ishii A, Sasaki N, *et al*. *J NeuroIntervent Surg* Epub ahead of print: [*please include* Day Month Year]. doi:10.1136/jnis-2024-022527

ABSTRACT

Background Bioresorbable flow diverters (BRFDs) have the potential to solve several problems associated with conventional permanent flow diverters. We have constructed bare and poly-L-lactic acid (PLLA)-coated magnesium BRFDs (MgBRFDs) using a high-strength corrosion-resistant magnesium alloy. This study aimed to compare bioresorption and biocompatibility between the two types in a rabbit vascular model to determine which is more clinically feasible in humans.

Methods Bare and PLLA-coated MgBRFDs were fabricated by braiding 48 thin magnesium alloy wires. Mechanical testing was conducted. Bare (n=13) and PLLA-coated (n=13) MgBRFDs were implanted into rabbit aortas and harvested 14, 30, and 90 days after implantation. The physical structure of the resolution process was examined using optical coherence tomography (OCT), micro-computed tomography, and scanning electron microscopy (SEM). The biological response of the vascular tissue was examined using SEM and histopathological analysis.

Results The porosity and pore density of the bare MgBRFD were 64% and 16 pores/mm^2, respectively; corresponding values for the PLLA-coated MgBRFD were 63% and 12 pores/mm^2, respectively. The OCT attenuation score was significantly higher for the PLLA-coated MgBRFD at all time points (14 days, P=0.01; 30 days, P=0.02; 90 days, P=0.004). OCT, micro-computed tomography, and SEM demonstrated better stent structure preservation with the PLLA-coated MgBRFD. Neointimal thickness did not significantly change over time in either type of MgBRFD (bare, P=0.93; PLLA-coated, P=0.34); however, the number of inflammatory and proliferative cells peaked at 14 days and then decreased.

Conclusions Both bare and PLLA-coated MgBRFDs had excellent biocompatibility. The PLLA-coated MgBRFD has greater clinical feasibility because of its delayed bioresorption.

WHAT IS ALREADY KNOWN ON THIS TOPIC

⇒ Bioresorbable flow diverters (BRFDs) can potentially solve the problems associated with conventional permanent flow diverters. Although magnesium is an excellent bioresorbable material, the development of a magnesium BRFD (MgBRFD) has been limited owing to magnesium's relatively low strength and rapid bioresorption.

WHAT THIS STUDY ADDS

⇒ This study demonstrated the in vivo absorption behavior and excellent biocompatibility of bare and poly-L-lactic acid-coated MgBRFDs. The coated type had delayed bioresorption and therefore has greater clinical feasibility in humans.

HOW THIS STUDY MIGHT AFFECT RESEARCH, PRACTICE OR POLICY

⇒ This study provides novel and important insights into the development of MgBRFDs.

INTRODUCTION

The introduction of flow diverters (FDs) for the treatment of unruptured intracranial aneurysms (IAs) has markedly improved patient outcomes.[1–4] However, currently available FDs, constructed using non-bioresorbable metals, pose long-term challenges such as potential complications from metal persistence. To address these issues, bioresorbable FDs (BRFDs) have been developed using several different types of absorbent material.[5–11] Magnesium is one of the best types of absorbent material for constructing FDs for several reasons. First, magnesium stents are more rigid than polymer ones and less susceptible to creep deformation (a process in which the stent slowly deforms owing to stress). Second, magnesium is antithrombotic as it degrades because of its electronegative charge.[12] Third, magnesium stents have already demonstrated excellent safety and biocompatibility in many clinical studies.[13 14]

Bioresorbable stent research has already been pioneered in the treatment of coronary artery disease. While bioresorbable polymer coronary stents have disappeared from the market because of in-stent thrombosis,[15] magnesium-based stents have advanced to the third generation of development. A recent study showed that a resorbable

magnesium stent achieved comparable 1-year outcomes to those of non-absorbable stents in patients with symptomatic coronary disease.[14] Thus, magnesium should be an appropriate material for use in BRFDs.

Despite this positive result, the development of magnesium BRFDs (MgBRFDs) has been hindered by material limitations. Two key challenges are magnesium's strength and its rapid absorption rate. Magnesium is weaker than cobalt chromium and nickel-titanium alloy; therefore, producing fine magnesium wire and braiding it to construct FDs is difficult. Its rapid bioresorption period is concerning because a MgBRFD may resorb before the aneurysm heals. In vitro resorption analysis of a MgBRFD in a 2023 proof of concept study showed complete resorption within 5 weeks,[8] highlighting the need for solutions to extend its resorption time

We have developed a magnesium alloy (KUMADAI Magnesium) using a rapidly solidified powder metallurgy process that features a distinctive long-period stacking-ordered structure. This alloy has shown superior strength, enhanced processability, and improved corrosion resistance compared with conventional magnesium alloys.[16–20] The unique properties of this alloy have enabled production of thin wires and the successful development of a MgBRFD. Because resorption time may be rapid according to previous research,[8] we have also developed a method for coating the magnesium wire with poly-L-lactic acid (PLLA) to improve corrosion resistance and lengthen resorption time. This study aimed to compare biocompatibility and bioresorption between PLLA-coated and uncoated (bare) MgBRFDs in a rabbit vascular model. Our ultimate goal was to determine which type of MgBRFD is more clinically feasible in humans.

METHODS

MgBRFD design and mechanical testing

The elemental composition of the magnesium alloy is shown in figure 1. The bare MgBRFD was created by weaving 48 magnesium alloy wires with a diameter of 46 µm (figure 1A–D). The thickness of the PLLA coating was 5 µm and the diameter of the coated wire was 56 µm. A high molecular weight PLLA (BMG, Kyoto, Japan) with a weighted average molecular weight of 220 000 g/mol was used as the PLLA coating. The diameter of both MgBRFDs was 4.0 mm. The stents were cut to the desired length for each experiment described below. Three radiopaque gold markers were attached to each end of the device.

Radial force testing and porosity and pore density assessment were performed in the two MgBRFDs as described in a previous study.[11] Radial force testing was also performed in an improved model of cobalt-chromium (CoCr) FD and a bioresorbable PLLA FD, which were developed in our previous research[11] for comparison.

In vivo animal experiments

The animal study protocol was approved by the Institutional Animal Care Committee of the Kyoto University Graduate School of Medicine (Med Kyo 21592, 23264). Twenty-six female New Zealand white rabbits (2.6–3 kg; Kitayama Labs, Ina, Japan) were used for the experiments.

MgBRFD implantation and harvesting

A study flow chart is shown in online supplemental figure 1. Animals were started on oral aspirin (30 mg/day) and clopidogrel (30 mg/day) 1 week before FD implantation, as previously described.[5 7 11] A single MgBRFD was implanted in the abdominal aorta of each rabbit via the right femoral artery (13 bare MgBRFDs in 13 rabbits and 13 PLLA-coated MgBRFDs in 13 rabbits). Balloon angioplasty was routinely performed to improve adherence to the vessel wall.

Rabbits were randomly sacrificed at 14, 30, and 90 days (n=4 at each time point). A 5 F sheath was inserted via the left femoral artery and optical coherence tomography (OCT; ILUMIEN OPTIS; Abbott Vascular, Santa Clara, California, USA) and angiography were performed. The rabbits were then euthanized and the vessels harvested. Further details are described in the online supplemental methods.

Element composition of Mg alloy

	Mg	Zn	Y	Al	Yb
at.%	balanced	0.9	2.05	0.15	0.1

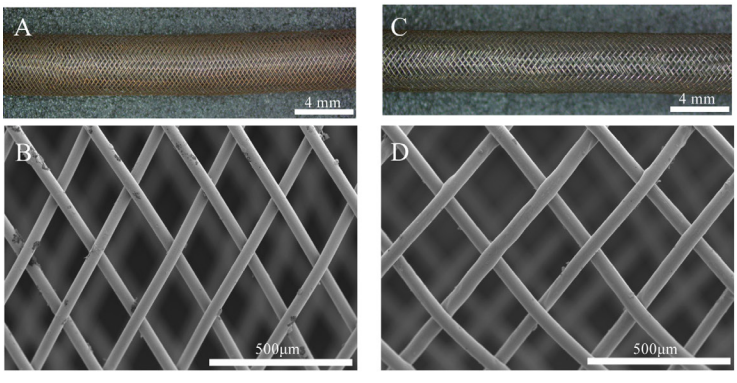

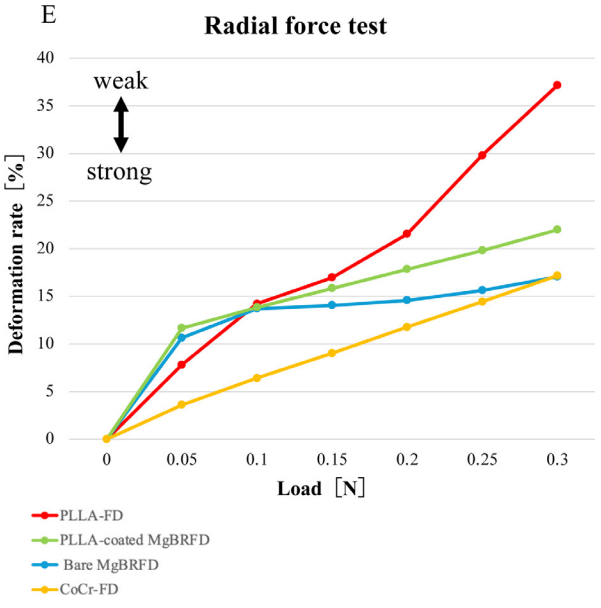

Figure 1 Structure and mechanical properties of magnesium-based bioresorbable flow diverters (MgBRFDs). Gross appearance and scanning electron microscopy images of the bare MgBRFD (A and B, respectively) and poly-L-lactic acid (PLLA)-coated MgBRFD (C and D, respectively). (E) Results of radial force testing of the PLLA flow diverter, PLLA-coated MgBRFD, bare MgBRFD, and cobalt-chromium flow diverter.

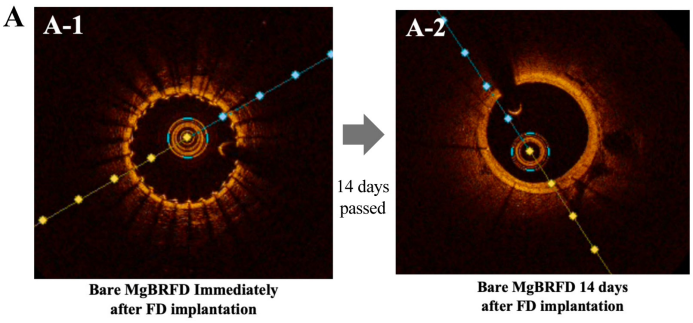

B

Attenuation score	OCT findings
2	Strut sharply delineated, complete attenuation behind strut
1	Strut diffusely delineated but no attenuation behind strut
0	No strut or attenuation behind the strut can be detected

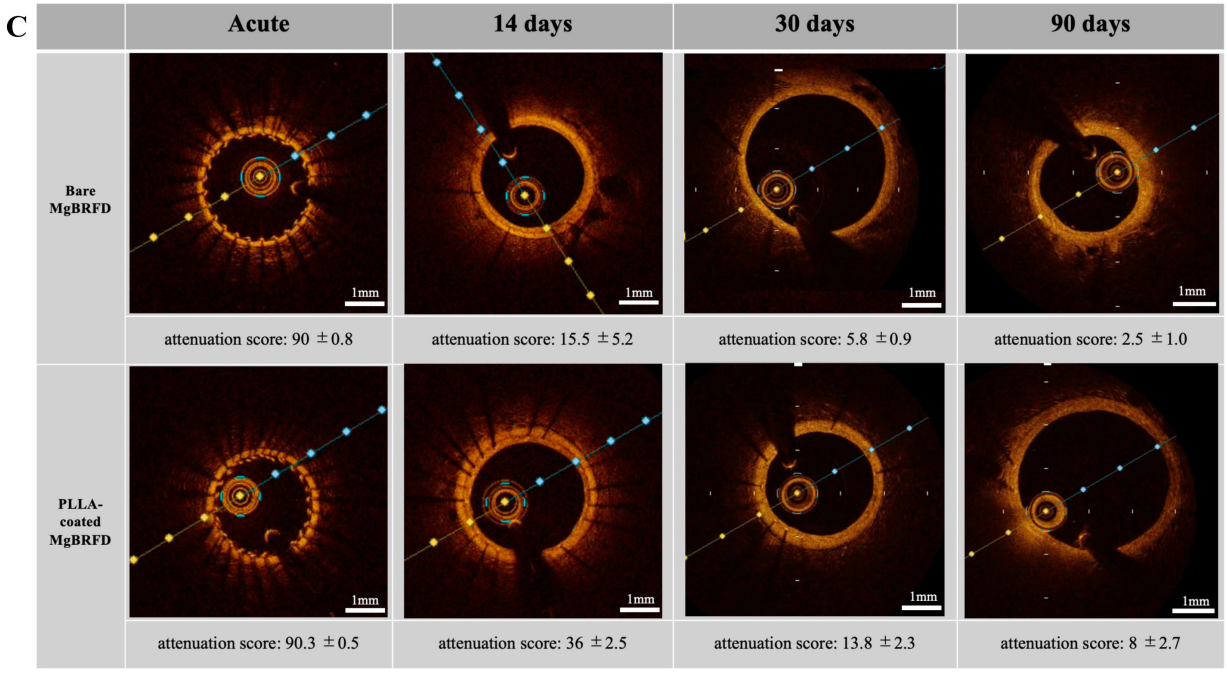

Figure 2 Optical coherence tomography (OCT) attenuation score. The OCT attenuation score was measured using the OCT cross-sectional view in the middle of the flow diverter. (A-1) Immediately after implantation, the stent struts are sharply delineated and backward attenuation is complete. (A-2) As degradation progresses, the stent struts and backward attenuation become obscured. (B) To quantify this change, the OCT attenuation score was calculated by summing the scores for each strut. (C) Scores and representative cross-sectional OCT images over time. Data shown are means±SE. At 14 and 30 days, the poly-L-lactic acid (PLLA)-coated magnesium-based bioresorbable flow diverter (MgBRFD) showed more stent struts and attenuation than the bare MgBRFD; therefore, attenuation scores were significantly higher in the PLLA-coated MgBRFD (P=0.01 at 14 days; P=0.02 at 30 days). At 90 days, attenuation scores remained significantly higher in the PLLA-coated MgBRFD (P=0.04); however, the absolute values were lower and stent struts were not visible in either the bare or PLLA-coated MgBRFDs.

Angiographic and OCT analysis

Angiography was performed before and after FD implantation and at follow-up to evaluate occlusion of the jailed lumbar artery. OCT was performed immediately after implantation and at follow-up to evaluate stent resorption, jailed microvascular patency, and in-stent stenosis. Because previous studies have shown that the OCT attenuation score correlates with magnesium stent bioresorption,[21] we calculated the original OCT attenuation score for the MgBRFD to evaluate its bioresorption. Attenuation scores were defined as follows: 2, strut sharply delineated, complete attenuation behind the strut; 1, strut diffusely delineated but no attenuation behind the strut; 0, no strut or attenuation behind the strut can be detected. The score was calculated by summing the scores for each strut on a cross-sectional view at the middle of the FD (figure 2A,B). Because the portion of the FD implanted along a branching vessel segment is the site most susceptible to degradation/resorption owing to continuous perpendicular blood flow, degradation/resorption was evaluated using OCT at that site (figure 3A). OCT was also used to evaluate the patency of small branching vessels (those smaller than 500 µm in diameter). Stent lumen stenosis was calculated as described in a previous study.[6]

Micro-CT (µCT) analysis

µCT was performed on selected MgBRFDs 0, 14, 30, and 90 days after implantation using a SkyScan 1172 scanner (Bruker, Kontich, Belgium) to evaluate preservation of the stent structure after embedding the specimens in paraffin (see online supplemental figure 1). Details of the imaging parameters are described in the online supplemental methods.

Scanning electron microscopy (SEM) and energy dispersive X-ray spectroscopy (EDX) analysis

SEM and energy dispersive X-ray spectroscopy (EDX) were performed on selected MgBRFDs 14, 30, and 90 days after implantation (n=1 or 2 per time point; online supplemental figure 1). Biocompatibility was evaluated by SEM observation of the neointimal coverage on the stent surface. Elemental analysis of the representative stent struts was performed on the central

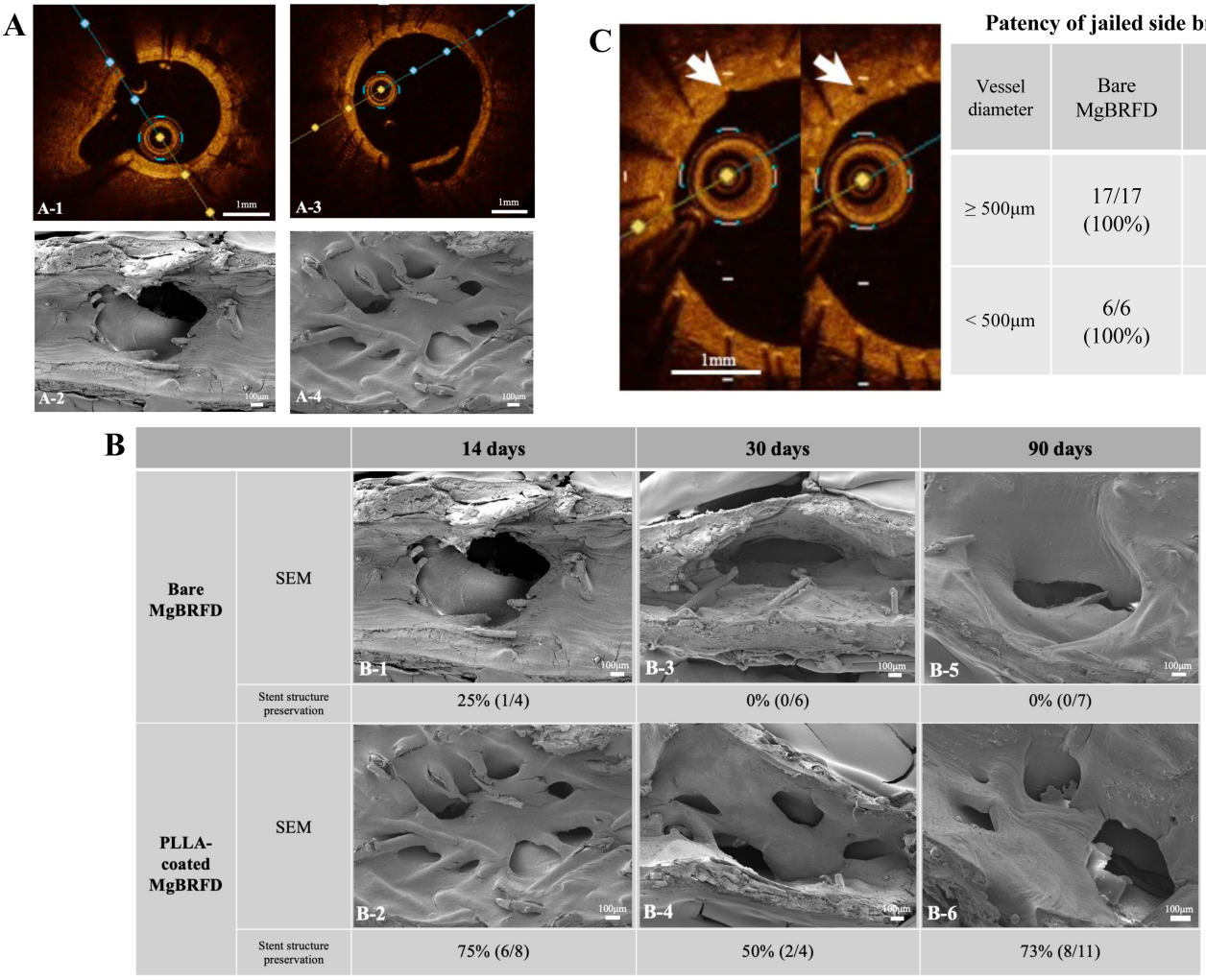

Figure 3 Resorption analysis of stent structures placed over side branches and patency of jailed side branches. Cross-sectional optical coherence tomography (OCT) images 14 days after implantation of a bare magnesium-based bioresorbable flow diverter (MgBRFD) (A-1) and a poly-L-lactic acid (PLLA)-coated MgBRFD (A-3) over a side branch. Corresponding scanning electron microscopy (SEM) images of the luminal surface of the vessel at the side branch site are shown in A-2 and A-4, respectively. The images clearly depict destruction or preservation of the stent structure at the site over the side branch. (B)Resorption analysis of stent structures at side branch sites using SEM and OCT images. SEM images at 14, 30, and 90 days after implantation are shown. Percentages indicate the preservation rate of the stent structure at each time point as depicted on OCT images. The stent structure at the side branch site was better preserved in the PLLA-coated MgBRFD at all time points. (C)Two consecutive OCT images show patency of a branch vessel approximately 100 μm in diameter (white arrowhead). The table on the right shows the percentage of jailed side branch patency according to vessel diameter.

cross-section of the stent using EDX to evaluate the degradation state and degradation products. Mapping analysis was performed on a representative stent strut. Eight representative stent struts were randomly selected and point analysis was performed at the center of each strut. SEM and EDX tissue processing and imaging details are described in the online supplemental methods.

Histopathological processing and analysis

Histopathological analysis was performed on selected MgBRFDs 14, 30, and 90 days after implantation (n=2 or 3 per time point; see online supplemental figure 1). Each harvested FD was divided into three sections (proximal, middle, and distal), and each cross-section was stained with hematoxylin and eosin, Elastica van Gieson, and Masson trichrome.

Immunohistochemical staining for ionized calcium binding adapter molecule 1 (Iba-1), Ki67, and alpha-smooth muscle actin (α-SMA) was also performed in the same section. Details of the processing and staining of histopathologic specimens are described in the online supplemental methods. Neointimal thickness measurements were performed as described in a previous report.[11] Cell counts of Iba-1-positive cells within the neointima were performed to assess local inflammation. Because Iba-1 could not stain giant cells infiltrating the stent struts, the percentage of stent struts infiltrated by giant cells was measured using hematoxylin and eosin staining as another assessment of local inflammation. Ki67 cell counts were performed to assess proliferative status within the neointima. α-SMA staining was performed to assess neointimal maturity. All measurements were performed in a blinded manner. Details of histopathological tissue processing and analysis are described in the online supplemental methods.

Statistical analysis

Statistical analyses were performed using JMP Pro 17 (SAS Institute, Cary, North Carolina, USA) or Prism 10 (GraphPad Software, San Diego, California, USA). Continuous variables

are expressed as means with SD and were compared using the unpaired two-tailed t-test or one-way ANOVA with Tukey's post-hoc test. Categorical data were compared using the χ^2 test or Fisher exact test. P<0.05 was considered statistically significant.

RESULTS

Physical and mechanical properties of MgBRFD

The porosity and pore density of the bare MgBRFD were 64% and 16 pores/mm^2, respectively; corresponding values for the PLLA-coated MgBRFD were 63% and 12 pores/mm^2, respectively. Radial force testing results are shown in figure 1E. The bare and PLLA-coated MgBRFDs were stronger than the PLLA-FD but weaker than the CoCr-FD.

Angiographic and OCT outcomes

Angiography showed patency of the lumbar artery at all time points in both types of MgBRFD (see online supplemental figure 2). OCT attenuation score results are shown in figure 2C. At all time points, OCT attenuation was significantly higher in the PLLA-coated MgBRFD (14 days, P=0.01; 30 days, P=0.02; 90 days, P=0.004). However, the absolute values of the attenuation score at 90 days were low for both types. Stent structure preservation over the origin of side branches is described in figure 3B. At all time points, stent structure was better preserved in the PLLA-coated MgBRFD. The overall structural preservation rates for the PLLA-coated and bare MgBRFDs were 73% and 5%, respectively. All small side branches <500 µm in diameter were patent in both types (figure 3C). Stent lumen stenosis on OCT was mild: the maximum for each type of MgBRFD was <10% (see online supplemental figure 3).

µCT outcomes

µCT results are shown in online supplemental figure 4. At 14 and 30 days, the bare MgBRFD exhibited more strut fractures.

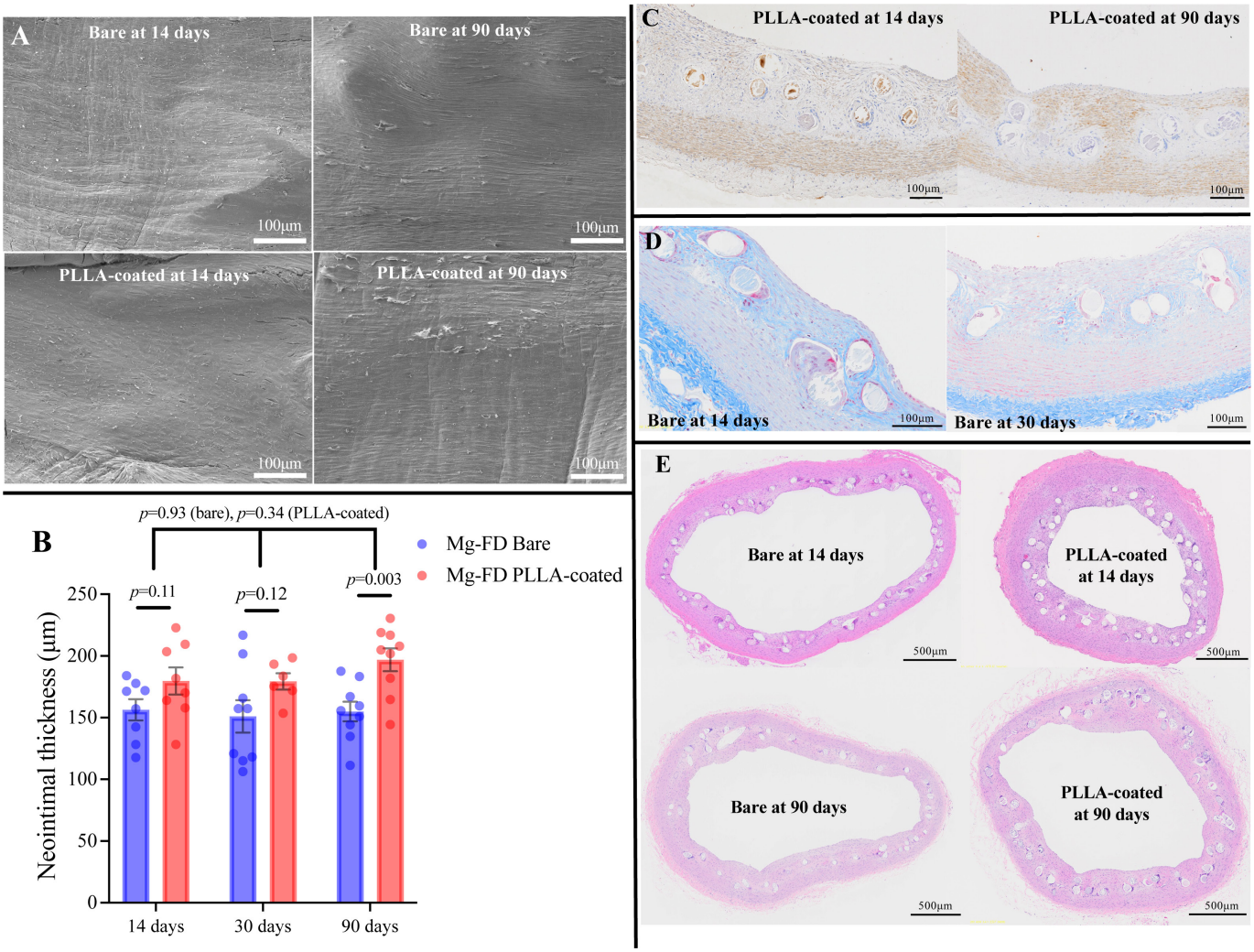

Figure 4 (A) Scanning electron microscope images of the luminal surface of implanted bare and poly-L-lactic acid (PLLA)-coated magnesium-based bioresorbable flow diverters (MgBRFDs). A smooth neointima covers the entire surface of both stents at 14 days; immature endothelial cells are observed to line up in a cobblestone pattern. Endothelial cells are fully mature and characterized by well-defined elongated cells aligned in the direction of flow. (B) Neointimal thickness over time. Dot plots show neointimal thickness per section. Data shown are means±SE. (C) Representative images of alpha-smooth muscle actin (α-SMA) immunoreactivity within the neointima at 14 and 90 days. Several α-SMA-positive smooth muscle cells infiltrated the neointima at 14 days and increased with time. (D) Cross-sectional histological images of an implanted bare MgBRFD at 14 and 30 days (Masson's trichrome stain). The extracellular matrix within the neointima was abundant at 14 days. At 30 days it decreased and infiltration of cellular components was observed. (E) Cross-sectional histological images of implanted bare and PLLA-coated MgBRFDs (hematoxylin-eosin stain).

At 90 days, a large extent of stent structure loss was observed in the bare MgBRFD but not in the PLLA-coated stent.

SEM and EDX outcomes

SEM images demonstrated excellent neointimal coverage of the entire luminal surface of each MgBRFD at 14 days (figure 4A). Excellent neointimal coverage was observed on the surface of the PLLA-coated MgBRFD's stent strut, even over the origin of the side branch where neointimal coverage is most difficult to achieve (figure 3B-2). The stent structure at the side branch sites was better preserved with the PLLA-coated MgBRFD (figure 3B).

EDX elemental analysis results are shown in figure 5 and online supplemental table 1. In the 14-day mapping analysis, magnesium was observed in the center of the stent strut only in the PLLA-coated MgBRFD. However, after 30 days it was almost unidentifiable in both types of MgBRFD. Decomposition to calcium proceeded similarly. The same trend was observed in the point analysis. The decomposition product of the magnesium alloy was presumed to be calcium phosphate.

Histopathological outcomes

Fourteen days after implantation, α-SMA-positive differentiated smooth muscle cells began to appear within the neointima in both types of MgBRFD and endothelial cells covered almost the entire surface of the neointima. Although the extracellular matrix (blue in Masson trichrome staining) comprised most of the neointima in both types at 14 days, the extracellular matrix decreased over time and a cellular component consisting of differentiated smooth muscle cells positive for α-SMA increased, indicating further neointimal maturation (figure 4C,D). The degree of neointimal maturation did not differ between the two types of MgBRFD.

The time course of neointimal thickness is shown in figure 4B,E and online supplemental table 2. Thickness did not significantly differ between the two groups at 14 and 30 days; however, the neointima was significantly thicker in the PLLA-coated group at 90 days (P=0.003). In both types, neointima thickness did not significantly change over time (bare, P=0.93; PLLA-coated, P=0.34).

Cell counts for Iba-1 and Ki67 and the percentage of stent struts infiltrated by giant cells are shown in figure 6 and online supplemental table 2. The number of Iba-1-positive cells was significantly higher in the bare MgBRFD group at 90 days (P=0.03) but not at other time points (14 days, P=0.64; 30 days, P=0.97). The number of Iba-1-positive cells significantly decreased over time in both groups (bare, P=0.04; PLLA-coated, P=0.005). The percentage of struts with giant cells significantly decreased over time in the bare MgBRFD group (30 days vs 90 days, P=0.008; 14 days vs 90 days, P<0.001). A similar trend was observed in the PLLA-coated MgBRFD group but the differences were not significant (P=0.12). Although the number of Ki-67-positive cells did not significantly differ between the groups at 14 and 30 days (14 days, P=0.06; 30 days, P=0.33), at 90 days the number was significantly higher in the PLLA-coated group (P=0.005). The number of Ki67-positive cells decreased significantly over time in the bare MgBRFD group (14 days vs 30 days, P=0.001; 30 days vs 90 days, P=0.002) and the PLLA-coated group (14 days vs 30 days, P=0.008; 30 days vs 90 days, P=0.02).

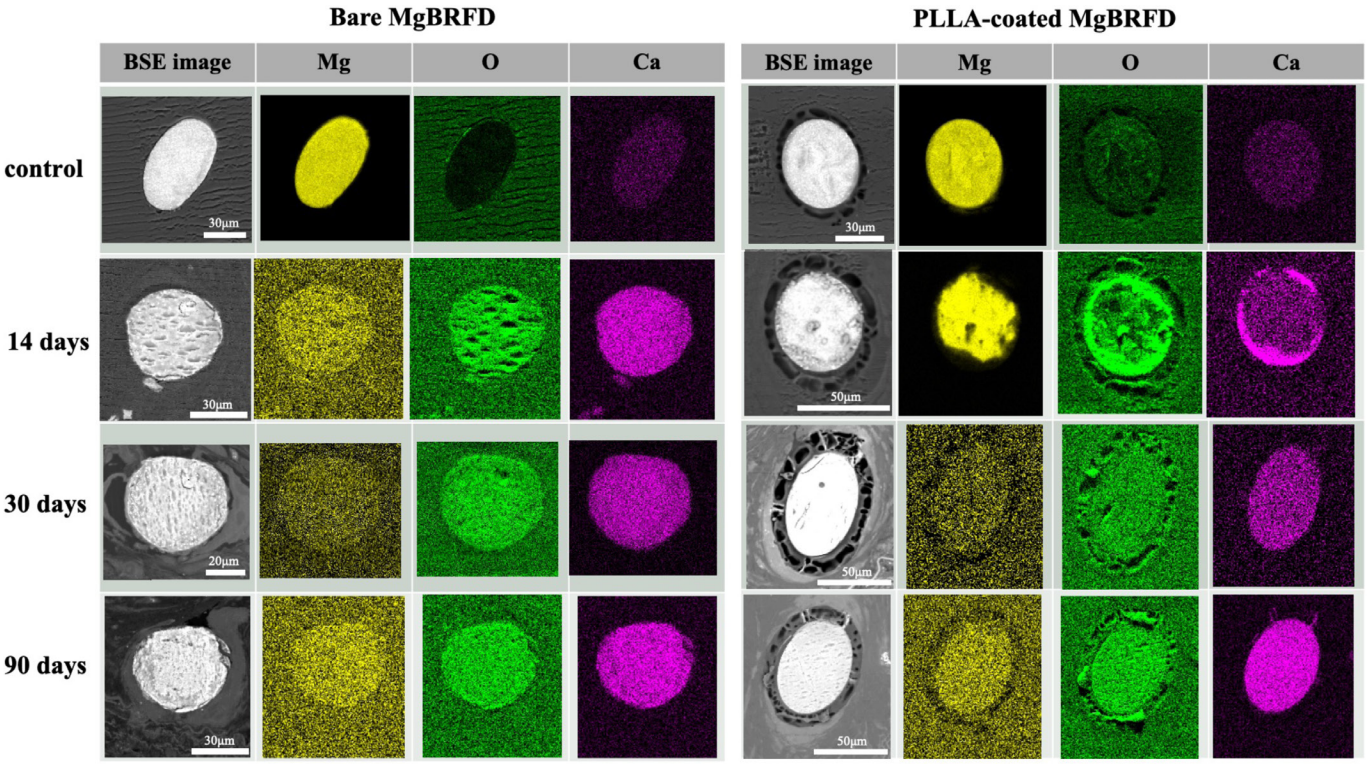

Figure 5 Energy dispersive X-ray spectroscopy mapping analysis results of representative stent strut cross-sections. At 14 days in the poly-L-lactic acid (PLLA)-coated magnesium-based bioresorbable flow diverter (MgBRFD), magnesium can be seen in most parts of the strut and there is a gradual change from the surrounding area to degradation products. In contrast, in the bare MgBRFD the magnesium concentration in the strut is almost the same as that in the background at 14 days and degradation products replace the entire strut. After 30 days, almost no magnesium is observed in either the bare or PLLA-coated stent struts and degradation products replace the entire strut. BSE, back scattered electron.

DISCUSSION

In this study of MgBRFDs in a rabbit vascular model, relatively mature neointimal coverage was achieved early, confirming their high biocompatibility. In addition, applying a PLLA coating prolonged their degradation. Previous studies of MgBRFDs in an animal aneurysm model used a coronary stent design, and these were completely different from the FDA-approved permanent FD design.[22 23] In an in vitro study of a MgBRFD designed by Oliver *et al*,[8] porosity was 81% and pore density was 4.3 pores/mm^2. These characteristics are far from ideal for achieving a sufficient flow diversion effect. In contrast, the porosity and pore density of our MgBRFD are equivalent to those of FDA-approved permanent FDs. To the best of our knowledge, this is the first study to confirm the in vivo reaction and resorption behavior of a MgBRFD that has a structure similar to that of conventional permanent FDs. Our findings should assist with further research and development of BRFDs, which may be the next breakthrough in endovascular treatment devices.

The initially reported BRFDs were constructed of PLLA, but more recent designs have used iron and magnesium alloys.[5–11] Metal BRFDs have several advantages over those constructed using a polymer. They are more rigid and have shown better mechanical performance in patients undergoing percutaneous coronary intervention.[24] Furthermore, magnesium stents have demonstrated excellent safety and biocompatibility in two clinical studies.[13 14] They also acquire an electronegative charge during degradation, which potentially confers antithrombotic properties.[12] However, rapid resorption is a problem with magnesium stents; the addition of a coating or adjustment of the alloy composition is required to delay the speed of resorption.

Although the resorption period of our MgBRFD was extended with a PLLA coating, it was still shorter than the 6–12 months required for a permanent FD to occlude an aneurysm. The elemental analysis showed that resorption without the coating was complete in 2 weeks. Even with the PLLA coating, the magnesium almost completely disappeared in 1 month. However, once the neointima had covered the stent structure, the covered degradation products appeared to remain as the stent structure. Therefore, the loss of an element does not necessarily indicate the loss of the stent structure. The ideal resorption period for BRFDs is the duration for which the stent structure remains intact until the aneurysm neck is covered with neointima. To evaluate the ideal resorption period of this MgBRFD, experiments implanting the device in an aneurysm model are required. A previous in vitro study of MgBRFD resorption reported markedly different results from ours.[8] Furthermore, in vitro and in vivo resorption times for magnesium stents can greatly differ,[25 26] possibly because replicating the complex in vivo conditions and environment in an in vitro circuit is quite difficult. Animal studies remain critical in mimicking magnesium resorption behavior in humans.

The thickness of the neointima covering both the bare and PLLA-coated MgBRFDs was greater than that reported in a previous study of PLLA and CoCr FDs.[11] However, it was similar to the thickness (100–200 µm) reported in preclinical studies of first- and second-generation FDs.[27 28] Moreover, stent lumen stenosis was only mild. Although we only examined neointimal thickness out to 90 days, we expect it to decrease beyond that time point because the number of proliferating and inflammatory cells in the neointima had been continuously

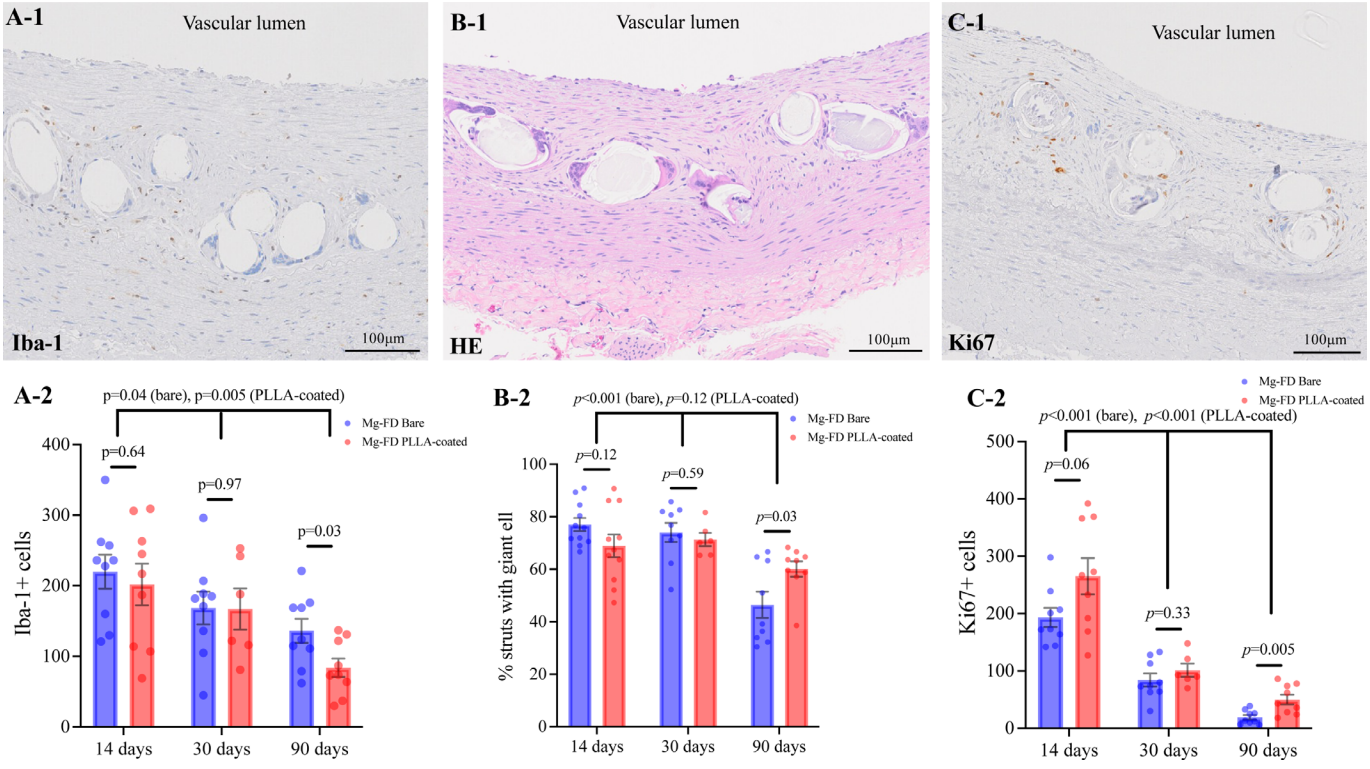

Figure 6 (A-1) Representative image of ionized calcium binding adapter molecule 1 (Iba-1) immunoreactivity in the neointima. (A-2) Cell counts for Iba-1-positive cells. Dot plots show Iba-1-positive cells per section. (B-1) Representative image of stent struts infiltrated by giant cells. (B-2) Percentage of struts with giant cells. Dot plots show the percentage of struts with giant cells per section. (C-1) Representative image of Ki67 immunoreactivity in the neointima. (C-2) Cell counts for Ki67-positive cells. Dot plots show Ki67-positive cells per section. Data in the graphs are means±SE.

decreasing in both the bare and PLLA-coated MgBRFD groups. Neointimal coverage of both MgBRFD types was rapid, with almost complete coverage of the stent surface at both the vessel wall and over the side branches at 2 weeks. Achieving coverage over the side branches is challenging because this site is not attached to the vessel wall and receives continuous blood flow in a perpendicular direction. Such remarkable neointimal coverage at side branch sites has not been observed with previous permanent FDs.[27–31] In fact, the side branch neointimal coverage of a PLLA-coated MgBRFD was clearly superior to that of a CoCr-FD, which was implanted in our previous research[11] (see online supplemental figure 5). If a MgBRFD can rapidly achieve adequate neointimal coverage, aneurysm occlusion should occur early and at a high rate. Therefore, a resorption period shorter than the estimated 6–12 months may be acceptable. Rapid neointimal coverage would also allow early discontinuation of antiplatelet therapy. The fact that excellent neointimal coverage is achieved even over side branches where the risk of thrombus formation is high is an additional strength of the MgBRFD. Further studies of PLLA-coated MgBRFDs in aneurysm animal models are needed, including ones comparing them with permanent FDs. Bare and PLLA-coated MgBRFDs rapidly achieved thick neointimal coverage without occluding branch vessels, including those <500 µm in diameter, confirming their safety.

Many inflammatory cells were present early in the neointima covering both bare and PLLA-coated MgBRFDs. A bare metal coronary stent study reported that the percentage of struts with giant cells was at most 20%,[32] which is considerably lower than the percentages found in our study for both types of MgBRFD. Therefore, the inflammatory response generated by the MgBRFD may be higher than that generated by permanent FDs. Previous porcine studies have reported that the inflammatory response is greater with resorbable magnesium coronary stents than permanent ones, which was attributed to the induction and activation of macrophages by magnesium degradation products.[25 33] The degradation/resorption rate of both types of MgBRFD is fast owing to its thin strut design, which presumably results in early induction of a greater number of inflammatory cells as degradation products accumulate. Macrophages play a pivotal role in neointimal formation,[34 35] and an early robust inflammatory response may explain why the MgBRFD induces excellent neointimal coverage. Early completion of magnesium resorption should reduce the neointimal inflammatory response over time; however, long-term data are needed to confirm this.

Limitations

This study has several limitations. First, we did not use a rabbit aneurysm model nor a permanent FD as a control. However, our device is a prototype, and our primary focus was to evaluate its feasibility. Second, the sample size was small. Third, the device needs improvement in several aspects. Despite the PLLA coating, resorption time was faster than expected and 30% of stent structures over side branches were not preserved. Improving the alloy composition as well as the method of coating may be required to prolong the resorption period further and prevent fragmentation due to stent degradation. Additionally, the device's radiopacity is inadequate, and thus we are considering combining it with a radiopaque material, as has been performed with other BRFDs. Furthermore, balloon angioplasty was routinely performed after device implantation because the apposition of the device to the vessel could not be confirmed under fluoroscopy. The introduction of radiopaque wires into the device is also anticipated to address this issue. Fourth, we did not evaluate whether embolization occurs with degradation-related device fragmentation. However, no large branch or peripheral vessel occlusions were observed. Finally, our observations were limited to 90 days after implantation. Long-term data are essential to confirm changes in neointimal thickness and inflammatory response and the final fate of the device's degradation products.

CONCLUSION

Both bare and PLLA-coated MgBRFDs had excellent biocompatibility in a rabbit vascular model. The PLLA-coated MgBRFD has greater clinical feasibility because the coating delayed bioresorption. Future validation studies are warranted.

Acknowledgements We thank the Kyoto Municipal Institute of Industrial Technology and Culture for µCT imaging and analysis and the Biopathology Institute Co Ltd. for pathology specimen preparation and imaging. We also thank the Institute of Laboratory Animals, Graduate School of Medicine, Kyoto University for animal management and Edanz (https://jp.edanz.com/ac) for editing a draft of this manuscript. Electron microscopy support was provided by the Division of Electron Microscopic Study, Center for Anatomical Studies, Graduate School of Medicine, Kyoto University.

Contributors Study conception: RA, AI, NS, SM, KI, SS, and YK. Data acquisition: RA, NS, SY, and SM. Data analysis: RA, AI, NS, SY, and SM. Interpretation and drafting the manuscript: RA, AI, NS, SM, and HC. Manuscript revision and final approval: all authors. RA and AI is responsible for the overall content as guarantor.

Funding This research was supported by the Japan Agency for Medical Research and Development (Grant number JP23he2202015).

Competing interests None declared.

Patient consent for publication Not applicable.

Ethics approval The animal study protocol was approved by the Institutional Animal Care Committee of the Kyoto University Graduate School of Medicine (Med Kyo 21592, 23264).

Provenance and peer review Not commissioned; externally peer reviewed.

Data availability statement Data are available upon reasonable request from the corresponding author.

ORCID iDs
Ryo Akiyama http://orcid.org/0000-0002-8700-3209
Akira Ishii http://orcid.org/0000-0003-4234-2749
Natsuhi Sasaki http://orcid.org/0000-0001-8206-3352
So Matsukawa http://orcid.org/0000-0002-1816-8632
Shinichi Yagi http://orcid.org/0009-0006-1689-803X
Hideo Chihara http://orcid.org/0000-0001-8767-6617
Hidehisa Nishi http://orcid.org/0000-0003-1763-2517
Kiyotaka Iwasaki http://orcid.org/0000-0002-3994-5509
Shinichi Sakurai http://orcid.org/0000-0002-5756-1066
Yoshihito Kawamura http://orcid.org/0000-0003-4823-9793
Yoshiki Arakawa http://orcid.org/0000-0003-4626-4645

REFERENCES

1 Brinjikji W, Murad MH, Lanzino G, *et al*. Endovascular treatment of intracranial aneurysms with flow diverters: a meta-analysis. *Stroke* 2013;44:442–7.
2 Kallmes DF, Brinjikji W, Cekirge S, *et al*. Safety and efficacy of the Pipeline embolization device for treatment of intracranial aneurysms: a pooled analysis of 3 large studies. *J Neurosurg* 2017;127:775–80.

3 Dandapat S, Mendez-Ruiz A, Martínez-Galdámez M, *et al*. Review of current intracranial aneurysm flow diversion technology and clinical use. *J Neurointerv Surg* 2021;13:54–62.
4 Hanel RA, Kallmes DF, Lopes DK, *et al*. Prospective study on embolization of intracranial aneurysms with the pipeline device: the PREMIER study 1 year results. *J Neurointerv Surg* 2020;12:62–6.
5 Wang K, Yuan S, Zhang X, *et al*. Biodegradable flow-diverting device for the treatment of intracranial aneurysm: short-term results of a rabbit experiment. *Neuroradiology* 2013;55:621–8.
6 Nishi H, Ishii A, Ono I, *et al*. Biodegradable Flow Diverter for the Treatment of Intracranial Aneurysms: A Pilot Study Using a Rabbit Aneurysm Model. *J Am Heart Assoc* 2019;8:e014074.
7 Jamshidi M, Rajabian M, Avery MB, *et al*. A novel self-expanding primarily bioabsorbable braided flow-diverting stent for aneurysms: initial safety results. *J Neurointerv Surg* 2020;12:700–5.
8 Oliver AA, Bilgin C, Vercnocke AJ, *et al*. Benchtop proof of concept and comparison of iron- and magnesium-based bioresorbable flow diverters. *J Neurosurg* 2023;139:150–6.
9 Oliver AA, Carlson KD, Bilgin C, *et al*. Bioresorbable flow diverters for the treatment of intracranial aneurysms: review of current literature and future directions. *J Neurointerv Surg* 2023;15:178–82.
10 Oliver AA, Koons EK, Trester PS, *et al*. Medical Imaging Compatibility of Magnesium- and Iron-Based Bioresorbable Flow Diverters. *AJNR Am J Neuroradiol* 2023;44:668–74.
11 Sasaki N, Ishii A, Yagi S, *et al*. Bioresorbable Poly (L-Lactic Acid) Flow Diverter Versus Cobalt-Chromium Flow Diverter: In Vitro and In Vivo Analysis. *Stroke* 2023;54:1627–35.
12 Rukshin V, Shah PK, Cercek B, *et al*. Comparative antithrombotic effects of magnesium sulfate and the platelet glycoprotein IIb/IIIa inhibitors tirofiban and eptifibatide in a canine model of stent thrombosis. *Circulation* 2002;105:1970–5.
13 Verheye S, Wlodarczak A, Montorsi P, *et al*. BIOSOLVE-IV-registry: Safety and performance of the Magmaris scaffold: 12-month outcomes of the first cohort of 1,075 patients. *Catheter Cardiovasc Interv* 2021;98:E1–8.
14 Haude M, Wlodarczak A, van der Schaaf RJ, *et al*. A new resorbable magnesium scaffold for de novo coronary lesions (DREAMS 3): one-year results of the BIOMAG-I first-in-human study. *EuroIntervention* 2023;19:e414–22.
15 Cassese S, Byrne RA, Ndrepepa G, *et al*. Everolimus-eluting bioresorbable vascular scaffolds versus everolimus-eluting metallic stents: a meta-analysis of randomised controlled trials. *Lancet* 2016;387:537–44.
16 Kawamura Y, Hayashi K, Inoue A, *et al*. Rapidly solidified powder metallurgy Mg97Zn1Y2 alloys with excellent tensile yield strength above 600 MPa. *Mat Trans* 2001;42:1172–6.
17 Abe E, Kawamura Y, Hayashi K, *et al*. Long-period ordered structure in a high-strength nanocrystalline Mg-1 at% Zn-2 at% Y alloy studied by atomic-resolution Z-contrast STEM. *Acta Mater* 2002;50:3845–57.
18 Yoshimoto S, Yamasaki M, Kawamura Y. Microstructure and Mechanical Properties of Extruded Mg-Zn-Y Alloys with 14H Long Period Ordered Structure. *Mater Trans* 2006;47:959–65.
19 Yamasaki M, Izumi S, Kawamura Y, *et al*. Corrosion and passivation behavior of Mg–Zn–Y–Al alloys prepared by cooling rate-controlled solidification. *Appl Surf Sci* 2011;257:8258–67.
20 Inoue S, Yamasaki M, Kawamura Y. Classification of high-temperature oxidation behavior of Mg-1 at% X binary alloys and application of proposed taxonomy to nonflammable multicomponent Mg alloys. *Corros Sci* 2020;174:108858.
21 Joner M, Ruppelt P, Zumstein P, *et al*. Preclinical evaluation of degradation kinetics and elemental mapping of first- and second-generation bioresorbable magnesium scaffolds. *EuroIntervention* 2018;14:e1040–8.
22 Nevzati E, Rey J, Coluccia D, *et al*. Biodegradable Magnesium Stent Treatment of Saccular Aneurysms in a Rat Model - Introduction of the Surgical Technique. *J Vis Exp* 2017;128:56359.
23 Grüter BE, Täschler D, Strange F, *et al*. Testing bioresorbable stent feasibility in a rat aneurysm model. *J Neurointerv Surg* 2019;11:1050–4.
24 Boeder NF, Dörr O, Koepp T, *et al*. Acute Mechanical Performance of Magmaris vs. DESolve Bioresorbable Scaffolds in a Real-World Scenario. *Front Cardiovasc Med* 2021;8:696287.
25 Wittchow E, Adden N, Riedmüller J, *et al*. Bioresorbable drug-eluting magnesium-alloy scaffold: design and feasibility in a porcine coronary model. *EuroIntervention* 2013;8:1441–50.
26 Menze R, Wittchow E. In vitro and in vivo evaluation of a novel bioresorbable magnesium scaffold with different surface modifications. *J Biomed Mater Res* 2021;109:1292–302.
27 Kallmes DF, Ding YH, Dai D, *et al*. A new endoluminal, flow-disrupting device for treatment of saccular aneurysms. *Stroke* 2007;38:2346–52.
28 Kallmes DF, Ding YH, Dai D, *et al*. A second-generation, endoluminal, flow-disrupting device for treatment of saccular aneurysms. *AJNR Am J Neuroradiol* 2009;30:1153–8.
29 Ding YH, Tieu T, Kallmes DF. Experimental Testing of a New Generation of Flow Diverters in Sidewall Aneurysms in Rabbits. *AJNR Am J Neuroradiol* 2015;36:732–6.
30 Starke RM, Thompson J, Pagani A, *et al*. Preclinical safety and efficacy evaluation of the Pipeline Vantage Embolization Device with Shield Technology. *J Neurointerv Surg* 2020;12:981–6.
31 Cortese J, Rasser C, Even G, *et al*. CD31 Mimetic Coating Enhances Flow Diverting Stent Integration into the Arterial Wall Promoting Aneurysm Healing. *Stroke* 2021;52:677–86.
32 Kornowski R, Hong MK, Tio FO, *et al*. In-stent restenosis: contributions of inflammatory responses and arterial injury to neointimal hyperplasia. *J Am Coll Cardiol* 1998;31:224–30.
33 Waksman R, Zumstein P, Pritsch M, *et al*. Second-generation magnesium scaffold Magmaris: device design and preclinical evaluation in a porcine coronary artery model. *EuroIntervention* 2017;13:440–9.
34 Rogers C, Welt FG, Karnovsky MJ, *et al*. Monocyte recruitment and neointimal hyperplasia in rabbits. Coupled inhibitory effects of heparin. *Arterioscler Thromb Vasc Biol* 1996;16:1312–8.
35 Pourdjabbar A, Hibbert B, Simard T, *et al*. Pathogenesis of neointima formation following vascular injury. *Cardiovasc Hematol Disord Targets* 2011;11:30–9.

Supplemental Materials

Magnesium-based bioresorbable flow diverter for intracranial aneurysms: a pilot study of biocompatibility and bioresorption in a rabbit vascular model

This document includes:

Supplemental Methods

Supplemental Figure 1-5

Supplemental Table 1-2

Supplemental Methods

MgBRFD implantation and harvesting

Rabbits were anesthetized using intravenous sodium thiopental (20 mg/kg) as an induction agent and maintained with 1%–2% isoflurane inhalation anesthesia. Local xylocaine was infiltrated at the skin incision site before sheath insertion. The femoral artery was exposed using the cutdown technique. A 4 F sheath was inserted and exchanged for a 5 F sheath before guiding a 0.014-inch wire to the thoracic aorta. Then, a MgBRFD was implanted through a 5 F catheter into the abdominal aorta. Angioplasty and OCT were performed via the same catheter.

Euthanasia was performed with an overdose of sodium thiopental (100 mg/kg) while under 1%–2% isoflurane inhalation anesthesia. Perfusion fixation and specimen harvesting were then performed as described in a previous study[11].

μCT analysis

Scans were acquired using a source voltage of 80 kV and source current of 100 μA through no filter. Projection images were taken every 0.2° over a 360° range with an exposure time of 0.8 seconds. Images were reconstructed and displayed using manufacturer-provided software (CTvox version 3.3.1; Bruker-MicroCT) to produce image data with a voxel resolution of 6 μm. Thresholding was based on the diameter of the magnesium wire prior to implantation.

SEM and EDX analysis

Tissue processing for evaluation of stent surface endothelialization by SEM was performed in the same manner as described in a previous study[11]. Tissue prefixation for EDX was performed similarly to SEM, creating a central cross-section of the vessel in which the FD was implanted. After post-fixation with 2% osmium tetroxide in distilled water at 4° C for 2 hours, the samples were dehydrated in a graded ethanol series(50%, 60%, 70%, 80%, 90%, 95%, 99%, and 100%) and treated with 100% propylene oxide followed by Epon 812. Specimens were prepared by embedding them in Epon 812 and cutting the cross-sections with a diamond knife. The samples were observed with a JSM-7900 scanning electron microscope (JEOL, Tokyo, Japan).

Histopathological processing and analysis

Histopathological processing was performed as described in a previous study[11]. Histopathological specimen preparation and hematoxylin and eosin staining, special staining, and immunohistochemical staining were outsourced to a specialized company (Biopathology Institute Co., Ltd, Oita, Japan). For

immunohistochemistry staining, the slides were blocked with skim milk and incubated with primary antibodies overnight at 4° C. Expression of the target molecules was visualized using 3,3'-diaminobenzidine (DAB) solution and nuclei were stained with hematoxylin. The primary antibodies were α-SMA polyclonal antibody, n-term (1:100; GeneTex, GTX89701), goat Iba-1 polyclonal antibody (1:100; Abcam, ab5076), and mouse Ki67 monoclonal antibody (1:100; Novus, NBP2-22112). Histopathological images were obtained using a Slideview VS200 Scanner (Olympus, Tokyo, Japan). Cell counts and neointima thickness were analyzed using the viewing software OlyVIA 4.1 (Olympus) and the BZ-X 800 analyzer (Keyence, Osaka, Japan).

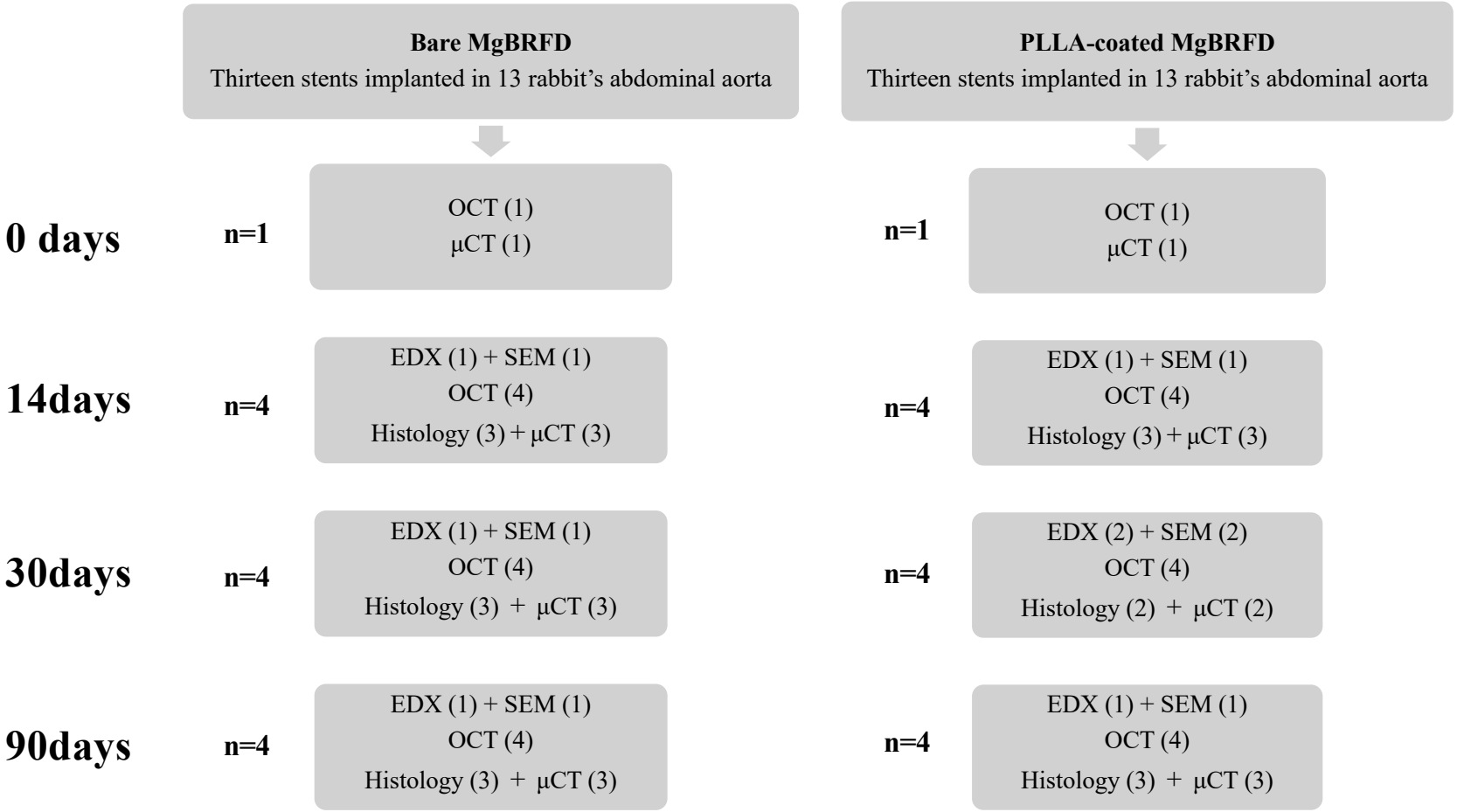

Supplemental Figure 1. study flow chart

Samples assigned for SEM and EDX analysis could not be used for histopathological analysis because the entire sample was required for SEM and EDX analysis. μCT could not perform samples assigned for SEM and EDX analysis due to the different tissue processing required. Due to an unexpected tissue processing failure on one sample of the PLLA-coated MgBRFD at 30 days, another sample was performed for EDX and SEM analysis.

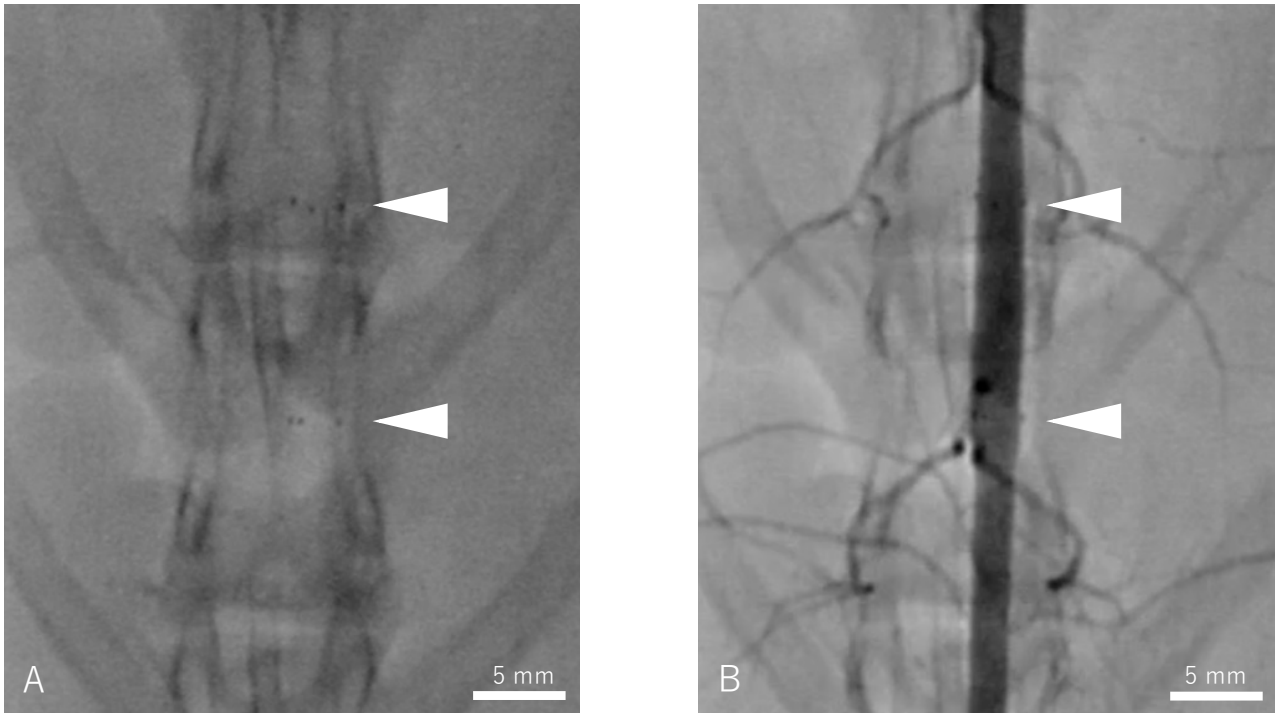

Supplemental Figure 2. Angiography 3 months after PLLA-coated MgBRFD implantation
A is a fluoroscopic image and **B** is an angiographic image. **A** shows that the stent is not radiopaque except for the radiopaque markers at both ends. **B** shows the patency of the aorta and its side branches covered by the stent. The white arrowheads indicate the radiopaque markers.

Follow-up	Device	Lumen area stenosis (%)
14 days	Bare	9.5 ± 0.8
	Coated	9.0 ± 0.6
	p-value	0.73
30 days	Bare	8.0 ± 0.8
	Coated	8.2 ± 0.4
	p-value	0.18
90 days	Bare	7.9 ± 0.3
	Coated	7.3 ± 0.5
	p-value	0.31

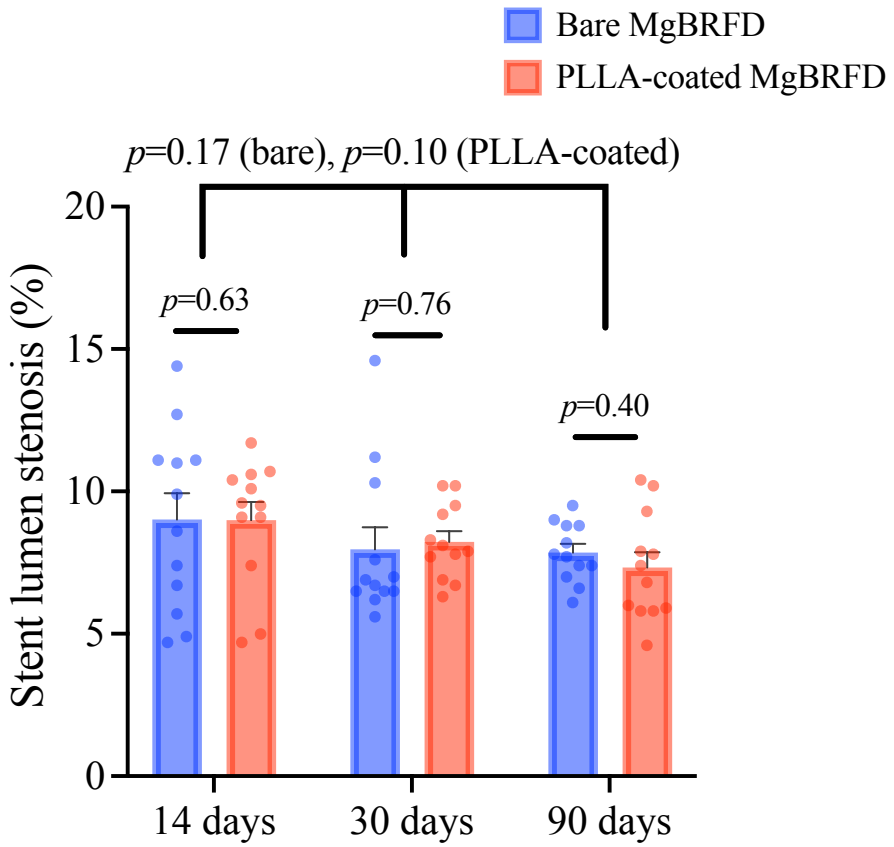

Supplemental Figure 3. Lumen area stenosis rate confirmed by OCT

There were no significant differences between stents at any time point and no significant changes over time for each stent. Analyses were performed using unpaired 2-tailed t test and 1-way ANOVA. Data are means ± standard error.

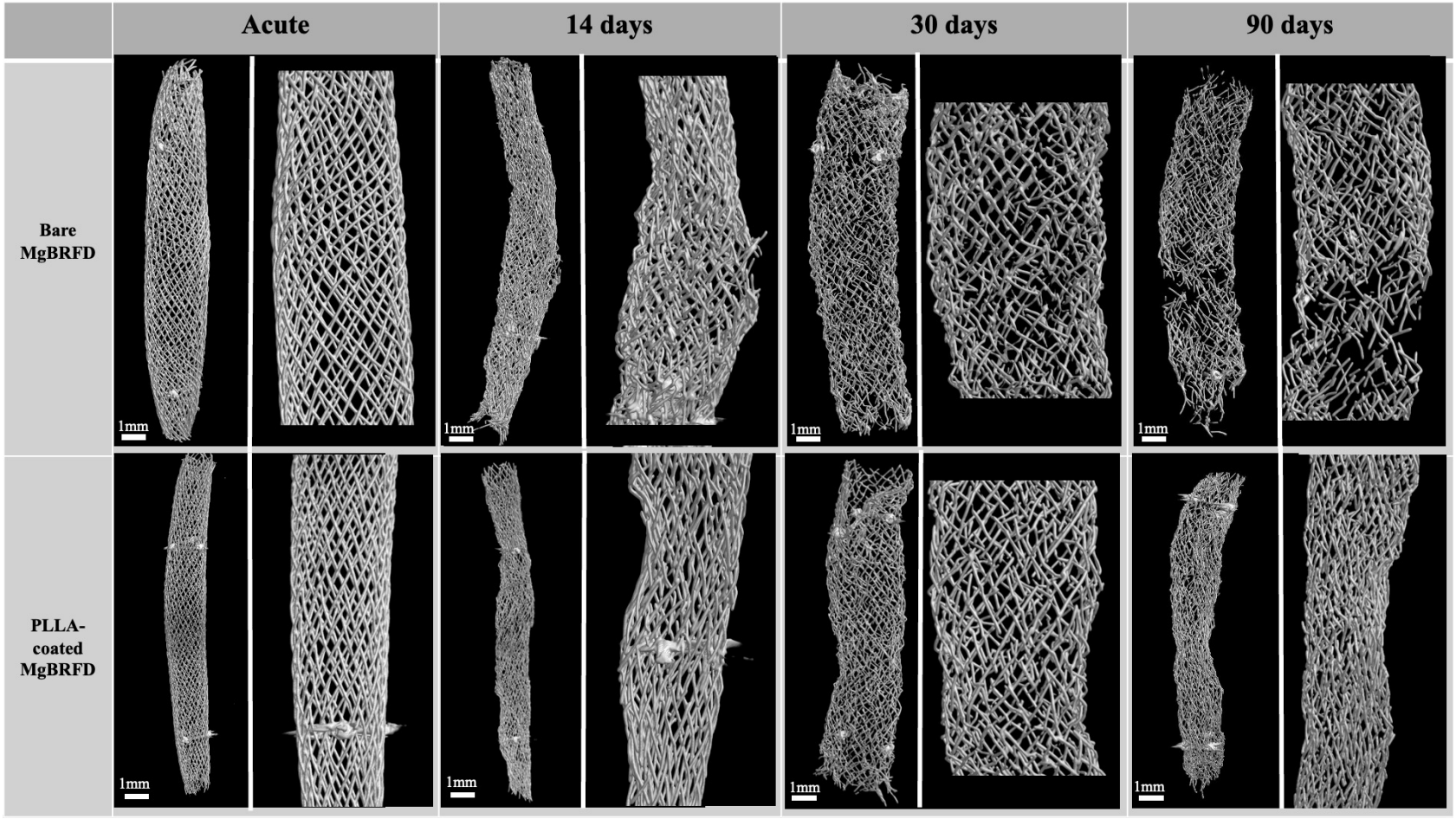

Supplemental Figure 4. μCT results over time for MgBRFDs

In each MgBRFD at each follow-up time point, the left side of the image is the whole image and the right side is a magnified image. At 14 days, bare MgBRFD showed the destruction of the stent structure over the side branch in the magnified image. At 30 days, bare MgBRFD showed more stent strut fractures in magnified images than PLLA-coated MgBRFD. At 90 days, bare MgBRFD showed areas of large stent structure loss.

	Control		14 days		30 days		90 days	
at.%	PLLA-coated	Bare	PLLA-coated	Bare	PLLA-coated	Bare	PLLA-coated	Bare
O	6.0±2.1	2.3±0.8	27.5±18.3	53.8±4.7	53.1±14.8	56.9±3.2	49.0±7.6	58.8±5.9
Mg	90.4±2.0	91.8±4.8	61.9±28.4	0.7±0.2	0.1±0.05	0.1±0.02	0.2±0.03	0.4±0.1
Al	0.3±0.04	0.3±0.05	0.4±0.2	0.6±0.1	0.4±0.1	0.5±0.1	0.3±0.04	0.3±0.1
P	0±0	0±0	4.3±7.0	23.6±2.2	26.1±7.5	20.8±1.6	24.2±3.4	19.8±2.7
Ca	0±0	0±0	1.3±2.0	10.9±2.2	8.81±3.6	11.9±1.9	16.7±3.7	13.1±2.4
Zn	1.0±0.1	1.4±0.8	1.7±1.2	2.8±0.8	2.0±1.3	1.8±0.3	1.1±1.9	0.7±0.3
Y	2.1±0.3	3.6±3.3	3.6±2.3	7.3±1.3	9.0±3.4	7.5±0.9	7.9±1.9	6.6±1.1
Yb	0.2±0.02	0.7±0.9	0.3±0.2	0.4±0.1	0.4±0.1	0.4±0.1	0.4±0.1	0.4±0.1

Supplemental Table 1. Point analysis results of the degradation products on the cross section of the MgBRFDs over time by EDX
Data are means ± standard deviation. The point analysis showed the same trend as the mapping analysis. Up to 14 days, More Mg elements remained in the PLLA-coated MgBRFD, but after 30 days, no difference was observed between the two MgBRFDs. The decomposition product of the Mg alloy is presumed to be calcium phosphate.

	14 days			30 days			90 days		
	Bare	PLLA-coated	p-value	Bare	PLLA-coated	p-value	Bare	PLLA-coated	p-value
Neointimal thickness (μm)	156 ± 5.0	180 ± 6.6	0.11	151 ± 7.1	179 ± 5.3	0.12	155 ± 5.7	197 ± 7.4	0.003
Iba-1 positive cells	220 ± 24.2	202 ± 29.5	0.64	168 ± 23.3	167 ± 29.1	0.97	136 ± 17.1	84 ± 13.0	0.03
Ki67 positive cells	193 ± 16.8	265 ± 31.6	0.06	84 ± 11.3	101 ± 11.5	0.33	19 ± 4.0	50 ± 8.5	0.005
% struts with Giant cell (%)	77 ± 2.5	69 ± 4.3	0.12	74 ± 3.6	71 ± 2.5	0.59	46 ± 5.0	60 ± 3.0	0.03

Supplemental Table 2. Histopathological Outcomes
Analyses were performed using unpaired 2-tailed t test. Data are presented as means ± standard error.

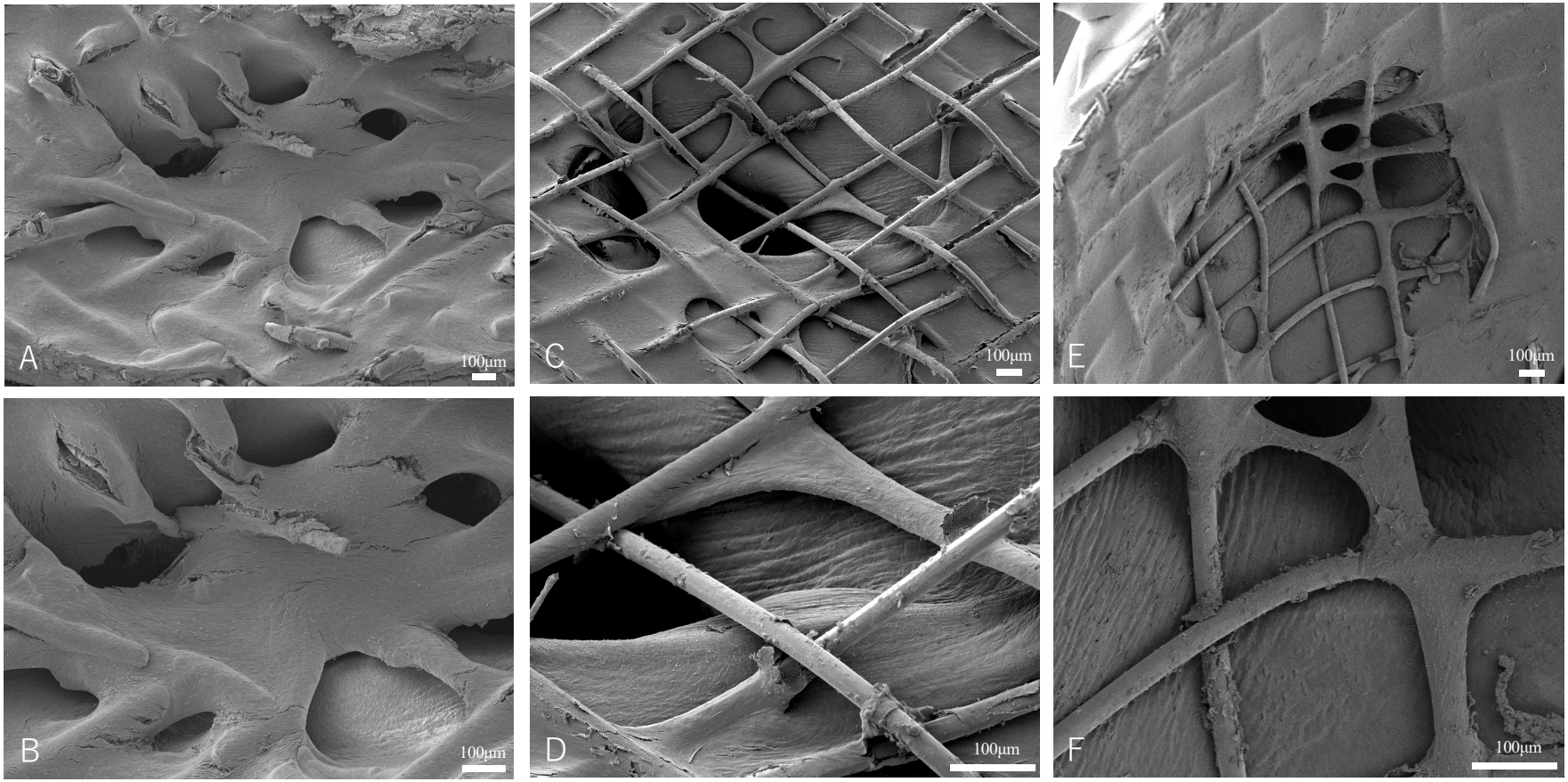

Supplemental Figure 5. Neointimal coverage of stent struts placed in the abdominal aorta over side branches (lumber arteries) on scanning electron microscopy
A and **B**) Neointimal coverage 14 days after implantation of low and high magnification PLLA-coated MgBRFDs, respectively. **C** and **D** show the neointimal coverage over the side branches 6 months after implantation of low and high magnification CoCr-FDs, respectively. **E** and **F** show the neointimal coverage over the side branches 24 months after implantation of low and high magnification CoCr-FDs, respectively. Compared to CoCr-FD, excellent intimal coverage is observed early, even over side branches where neointimal coverage is difficult to achieve with MgBRFD.